JOURNAL OF GEOPHYSICAL RESEARCH: SPACE PHYSICS, VOL. 118, 1–10, doi:10.1002/jgra.50183, 2013

Orientation of solar wind dynamic pressure phase fronts

Brian J. Jackel,[1] Taylor Cameron,[1] and James M. Weygand[2]

Received 1 October 2012; revised 12 January 2013; accepted 9 February 2013.

[1] Orientation of structures in the solar wind plays an important role when attempting to use upstream observations at L1 for prediction of subsequent conditions near the Earth. In this study, the relationship between solar wind dynamic pressure forcing and geosynchronous magnetic field response is used to determine a very large set of lagged correlations between the ACE and GOES satellites. Effects due to tilted solar wind structures are explored using the dispersion of arrival times relative to a simple phase plane model. Assuming that structure phase-front normal vectors were located in the GSE-*xy* plane, we found a characteristic azimuth of 15°. Similar analysis carried out with velocity scaling according to the Parker spiral model did not produce an improved fit. Binning by average interplanetary magnetic field (IMF) $\vec{B}$ orientation produced a clear pattern in characteristic azimuth, with phase-front normals perpendicular to both the predominant Parker spiral orientation and the less common ortho-spiral configuration. An empirical relationship $\phi_{\hat{n}} = -45° \sin(2\,\phi_B)$ was found to predict phase-front normal azimuth over the entire range of observed IMF azimuths. The effects of lateral displacement from the Sun-Earth line in the GSE-*z* direction are comparable to those for GSE-*y*, indicating that solar wind structures are often significantly inclined with respect to the ecliptic plane.

Citation: Jackel, B. J., T. Cameron, and J. M. Weygand (2013), Orientation of solar wind dynamic pressure phase fronts, *J. Geophys. Res. Space Physics*, *118*, doi:10.1002/jgra.50183.

1. Introduction

[2] A dynamic and highly structured geospace environment is produced by complex interactions between the solar wind and the terrestrial magnetic field. The behavior of this geospace system can be used to study fundamental processes of plasma physics. It is also of practical importance due to the potentially damaging effects on technology in space and at the Earth's surface. Large variations in the solar wind magnetic fields and particle populations are ubiquitous, due primarily to temporal and spatial variations near the solar surface. Many important magnetospheric processes are influenced by changes in the solar wind, so a detailed knowledge of solar wind forcing would be essential to a complete understanding of magnetospheric response. However, information about the solar wind state is generally only available from a small number (often one) of satellites making point measurements at relatively distant upstream locations. A variety of algorithms have been developed for propagation of such distant observations to the magnetopause. In this study, we introduce a novel approach for testing these algorithms using a combination of solar wind dynamic pressure and geosynchronous magnetic field data.

2. Time Shifting

[3] In order to study magnetospheric response to solar wind forcing, it would be ideal to have an upstream platform that is relatively close to the Earth. This would provide accurate measurements of the solar wind just prior to any interactions with the bow shock or magnetopause. For space weather forecasts, it would be preferable to acquire observations from a platform located closer to the Sun, as that would allow for early warning of conditions that may pose a risk to technology or human health. However, conditions observed by a distant upstream monitor may be different than those that arrive at the Earth, either due to spatial inhomogeneity or temporal changes in the plasma during propagation.

[4] Constraints due to orbital mechanics also require a choice between two classes of orbits: Earth centered with apogee upstream of the bow shock (e.g., IMP-8) or a halo orbit near the L1 Lagrange point (e.g., ISEE-3). Geocentric orbits produce coverage gaps when the spacecraft is traveling through the magnetosphere. Maintaining a stable orbit near L1 requires careful attention but can provide a continuous monitor of the upstream solar wind. Recent missions have used the L1 option (e.g., Wind, ACE) to provide solar wind observations from locations 200 or more Earth radii (Re) closer to the Sun.

[5] The instantaneous heliospheric magnetic field near L1 often resembles a colored random process on short (1 h)

[1]Physics and Astronomy Department, University of Calgary, Calgary, Alberta, Canada.
[2]Department of Earth and Space Sciences, University of California, Los Angeles, California, USA.

Corresponding author: B. J. Jackel, Physics and Astronomy, University of Calgary, 2500 University Drive, NW, Calgary, Alberta, Canada T2N 1N4. (bjackel@ucalgary.ca)

2169-9380/13/10.1002/jgra.50183

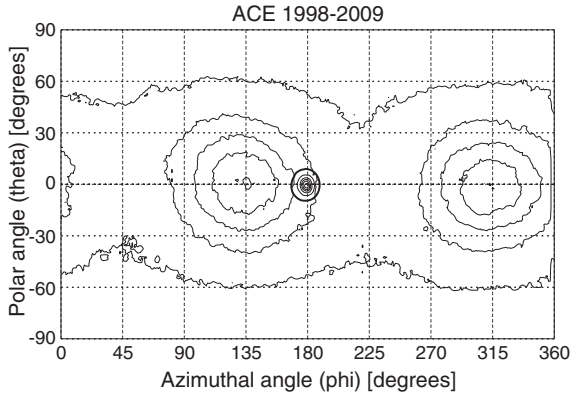

Figure 1. Orientation of solar wind observed by ACE 1998–2009. Thick contours correspond to distribution of magnetic field direction normalized to 10, 30, 50, 70, and 90% of the most probable value. Thin contours centered on $\phi = 180°$ and $\theta = 0°$ correspond to the observed velocity distribution which is predominantly antisunward; very thick contour indicates 1% likelihood.

time scales. A compilation of observations over a year or longer will however exhibit certain patterns that only emerge in a statistical sense. Figure 1 contains the angular distribution of 1 min average $\vec{B}$ measured by ACE [*Smith et al.*, 1998] from 1998 to 2008. Magnetic fields are typically inclined close to the equatorial plane ($|\theta_B| < 30°$) with a strong preferential azimuthal alignment near $\phi = 135°$ and $\phi = 315°$. These preferred directions correspond to the well-known Parker spiral [*Parker*, 1965]

$$\tan\alpha_P = \frac{B_\phi}{B_r} = \frac{\Omega\, r}{v} \approx \frac{400\ \text{km/s}}{v} \tag{1}$$

where Ω is the angular velocity of the Sun, v is the radial plasma speed, r is the radial distance (1 AU), and α_P is the spiral pitch angle ($\phi = 180° - \alpha$). For typical values of $v \sim$ 400 km/s, the Parker spiral angle of $\alpha_P \sim 45°$ agrees very well with the results in Figure 1.

[6] Given solar wind data from near L1, the usual objective is to predict what will arrive at the Earth's magnetopause more than an hour later. This is potentially a very hard problem for an arbitrary plasma with a range of spatial scales all evolving differently with time. Fortunately, it has been shown [*Richardson and Paularena*, 1998; *Ogilvie et al.*, 2007] that the solar wind is typically dominated by spatial scales greater than 100 Re that are fairly coherent over time scales of an hour.

[7] It is customary to assume that any relatively stable large-scale structures are embedded in the background plasma and consequently move with bulk velocity vector $\vec{v}$. This is equivalent to neglecting any effects due to dispersive wave propagation and drastically simplifies the problem, as measured solar wind flows are dominated by the radial outward component. Figure 2 shows the distribution of the antisunward component observed by the ACE SWEPAM instrument [*McComas et al.*, 1998] during nearly a solar cycle spanning 1998–2008. There is clearly considerable variation from year to year, with higher-speed streams more likely during the declining phase after solar maximum. Similar variability exists over a wide range of time

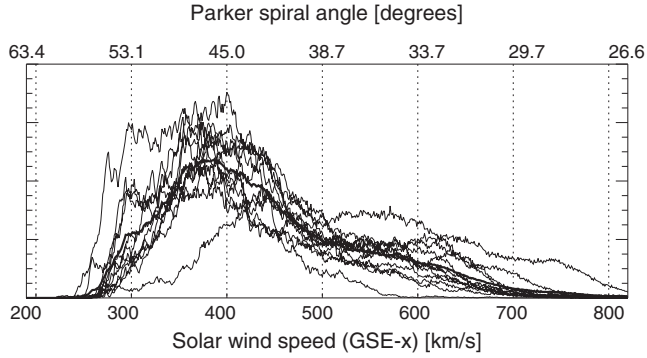

Figure 2. Yearly distributions of solar wind speed observed by ACE from 1998 to 2009. Thick line corresponds to average over all years.

scales extending down to the range of interest for this study (several hours). Time-resolved velocity measurements are thus critical for any attempt at propagating L1 observations to the Earth. Of course, the solar wind velocity field also varies in space, so that upstream measurements must be made from locations very near to the Sun-Earth line. If the solar wind probe is offset laterally (i.e., GSE-y and/or GSE-z) by a significant amount, then it will be on a streamline that traces to a location offset from the Earth's bow shock "nose" or, worse, passes by the magnetosphere entirely. In this case, additional assumptions are required to extrapolate beyond the available observations.

[8] Further progress typically involves the assumption that solar wind spatial structures can be modeled by large-scale "phase fronts" [*Kelly et al.*, 1986; *Blanchard and Bankston*, 2002; *Weimer and King*, 2009] which are approximately planar. This extremely simple model often provides a good fit for two-point observations, although as noted by *Weimer et al.* [2002]: "the planar phase fronts are certainly approximations to large-scale, curved or undulating structures in the IMF." Moving beyond a planar model requires the use of data from three or more spacecraft separated by moderate (10–50 Re) distances, which happens very rarely. Such conjunctions have been used by *Weimer et al.* [2002], who found that the planar model agreed well with data from four satellites, while a multisatellite study by *Lepping et al.* [2003] estimated the typical radius of curvature to be roughly 300 Re.

[9] It can be shown (see Appendix A) that a plane with normal $\hat{n}$ moving at velocity $\vec{v}$ will be observed by two different satellites with a time difference

$$\Delta t = t_2 - t_1 = \frac{\left[\vec{r}_2 - \vec{r}_1\right] \cdot \hat{n}}{\vec{v} \cdot \hat{n}} \tag{2}$$

that depends on the location $\vec{r}_1$ of the first observer at time t_1 and the velocity $\vec{v}_2$ of the second observer located at $\vec{r}_2$ at time t_2.

[10] If the phase plane velocity is predominantly antisunward $\left(\vec{v} = -v\hat{x}\right)$, then the time shift can be approximated

$$-\Delta t \approx \frac{\Delta x}{v} + \frac{\Delta y}{v}\tan\phi + \frac{\Delta z}{v}\frac{\tan\theta}{\cos\phi} \tag{3}$$

as a function of the offset between the two observation locations ($\Delta x = x_2 - x_1$, $\Delta y = y_2 - y_1$, $\Delta z = z_2 - z_1$), the solar

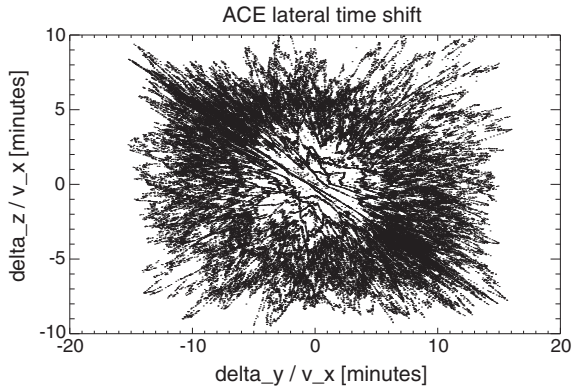

Figure 3. Hypothetical lateral time shifts from a decade of ACE observations, assuming phase-front normal azimuth $\phi = 45°$ and inclination $\theta = 35°$. These are $\Delta y/v$ and $\Delta z/v$ relative to $\vec{r}_2 = 0$, with spatial offsets due to an elliptical orbit in the y-z plane and v as the hourly average solar wind speed. This effect will vanish if $\phi = 0$ and $\theta = 0$.

wind speed v, and the phase plane normal (PFN) orientation $\hat{n} = \{x_n, y_n, z_n\}$ in terms of the azimuth ϕ and inclination θ (antisunward flow in the ecliptic plane corresponds to $\phi = 180°$ and $\theta = 0$).

[11] When $\phi = 0$, the phase-front normals are aligned with GSE-x for structures that are uniform with constant radial distance from the Sun. In this case, the "flat" time shift depends only on the upstream distance Δx and the solar wind speed. During 1998–2008, the ACE upstream distance was fairly constant ($\Delta x = 220$–250 Re), but large variations in solar wind speed produced a wide range of flat time shifts ($\Delta t_x \approx$ ~~30~~–90 min). Of course, the PFN azimuth and inclination are not necessarily zero, introducing lateral ("tilted") time shifts from the last two terms in equation (3). The magnitude of these tilt effects depends on the specific azimuth and inclination, but a useful estimate of their importance can be obtained by assuming that the trigonometric terms are of order 1. Results for the ACE spacecraft from 1998 to 2009 are presented in Figure 3. The actual orbital displacements followed a precessing elliptical pattern in the range $\Delta y = \pm 40$ Re and $\Delta z = \pm 25$ Re; when divided by the solar wind speed, the resulting tilted time shifts are $|\Delta t_y| \approx 15$ min and $|\Delta t_z| \approx 10$ min.

[12] Calculation of the actual lateral time shift requires accurate values of θ and ϕ. The general problem of determining phase-front orientation has received considerable attention [e.g., *Ridley*, 2000; *Mailyan et al*., 2008] but is still an active research topic. Popular approaches include using a single nominal orientation (i.e., flat or Parker spiral), the instantaneous or average magnetic field ($\vec{B}$) orientation, cross products of $\vec{B}$ across a discontinuity, basic principal component analysis, and various hybrid techniques. For this study, we will focus on the first two approaches in order to maintain a reasonable scope.

3. Analysis

[13] Studies of time-shifting algorithms typically involve a direct comparison of some physical parameter measured by two satellites that are both in the solar wind. Such an approach requires a search through multiple data sets in order to identify intervals with two (or more) conveniently located spacecraft, usually providing few hundred or thousand intervals of comparable data. This has proven sufficient for the development of existing time-shifting algorithms, but further improvements would certainly benefit from the availability of larger data sets.

[14] For this study, we have compared two different (but related) physical quantities: dynamic pressure $\left(P_d = nv^2\right)$ in the solar wind and the GSM-z component of magnetic field (B_z) at geostationary orbit. Sudden impulses in P_d are known [*Siscoe et al.*, 1968] to produce step-function increases in B_z; a similar relationship exists between sinusoidal forcing and response [*Kepko et al.*, 2002]. A recent study by *Jackel et al.* [2012] further explored the statistical relationship between arbitrary variations in P_d and subsequent changes in B_z. They found that when GOES was located on the dayside, there was a significant correlation between geosynchronous B_z and upstream P_d approximately 25% of the time. This provides an opportunity to obtain a very large number of conjunctions, as all observations from a single solar wind probe can be compared to each GOES platform (two are usually operational at any given time [*Singer et al.*, 1996]).

[15] In *Jackel et al.* [2012], the solar wind dynamic pressure was obtained from the widely used high-resolution OMNI compilation (HRO) derived from several different sources [*King and Papitashvili*, 2010]. The HRO OMNI data have been time shifted using a state of the art hybrid algorithm [*Weimer and King*, 2009] based on the model of convecting phase planes. In this study, we use solar wind data from the ACE spacecraft [*Stone et al.*, 1998] focusing on observations from particle and magnetic field instruments. These data have not undergone any propagation corrections, allowing us to use them to explore various aspects of the phase plane model.

3.1. ACE Solar Wind

[16] The calibrated solar wind data used in this study was measured by ACE SWEPAM [*McComas et al.*, 1998] and MFI [*Smith et al.*, 1998] and downloaded from http://cdaweb.gsfc.nasa.gov. SWEPAM data were provided at 64 s resolution and the MFI data at 16 s resolution. To obtain a uniform data set, we linearly interpolated the data to 1 min resolution. We interpolate across gaps of 10 min or less; larger gaps are filled with flags and avoided in subsequent analysis.

3.2. GOES Magnetometers

[17] Observations from instruments on the Geostationary Operational Environmental Satellite (GOES) are used by the NOAA Space Weather Prediction Center for the real-time monitoring and prediction of the conditions in the Earth's space environment [*Singer et al.*, 1996]. Two satellites are typically operational at any given time, located near 135° and 75° geographic west longitude, respectively. A wide variety of data are collected by different sensors, including in situ measurements of the magnetic field and energetic particles. For this study, we used publicly available key parameter data including 1 min averaged vector magnetic field values provided in GSM and several other coordinate

systems. Instrument quality data flags were also used to identify gaps and other problematic samples which were excluded from analysis.

3.3. Lagged Correlation

[18] Data analysis involved the lagged correlation between solar wind dynamic pressure and geosynchronous magnetic field. Details are given below, based on the procedure used by *Jackel et al.* [2012], which contains additional discussion and motivation for the various steps used here. Lagged correlation analysis can be used to identify the conditions which produce the best match between changes in solar wind dynamic pressure and the response in geosynchronous B_z. We assume that solar wind density structures can be approximated as phase planes that move with the bulk velocity (v_x) and remain coherent over the time scales of interest (i.e., 1 h). For this study, we are particularly interested in effects related to phase plane orientation.

[19] Starting with a 1 h (60-sample) interval of solar wind data, the average velocity was used to calculate the "flat" delay $\Delta t_x = \Delta x/v$ from the L1 platform location to the GSE origin. All subsequent consideration of lag τ is with respect to this flat shifted time:

$$\tau_{yz} \approx \leftarrow \Delta t - \frac{\Delta x}{v} = \frac{\Delta y}{v}\tan\phi + \frac{\Delta z}{v}\frac{\tan\theta}{\cos\phi} \tag{4}$$

[20] A 4 h (240-sample) interval of GOES B_z (GSM) centered on the flat delay time was detrended using a second-order polynomial in order to remove effects due to satellite motion through spatially varying fields (i.e., stronger average magnetic fields on the dayside). The detrended data were used to calculate correlation coefficients at a range of lags from –90 to +90 min relative to the flat delay time. This interval was selected to be sufficient so as to include the majority of tilt-based shifts for ACE up to $\phi = \pm 80°$. Any tilt larger than this will produce extreme delays that will not be identified by our correlation analysis.

[21] The process was repeated for the next solar wind segment which was shifted by half the interval (30 min) in order to ensure that distinct features (e.g., pressure pulses) would occur near the middle of at least one interval. Intervals with more than 10% gaps in either data segment were discarded; all others were included in subsequent analysis. The "peak" (largest positive) correlation coefficient was identified and stored along with the corresponding lag and averages of various physical quantities including average magnetic field vector.

[22] For two sets of values drawn from independent Gaussian distributions ("white" noise), it would be possible to accurately model the distribution of sample correlation coefficients. However, like many geophysical time series, both data sets studied here exhibit a considerable amount of auto-correlation. The distribution of cross-correlations for this kind of "colored" noise is difficult to model accurately, but it will tend to produce much higher values than would be expected for Gaussian processes. An empirical comparison [*Jackel et al.*, 2012] using acausal comparisons (geosynchronous variation preceding solar wind changes) as a reference showed that the distribution of "signal" peak sample correlations has considerable overlap with the "noise" distribution. One response to this ambiguity would be to require an extremely high threshold (i.e., $r > 0.9$) for acceptable correlations, but this would result in the rejection of a very large number of events that were actually causally related.

[23] A useful alternative is to discriminate on the basis of lag time. Consider two uncorrelated colored noise sequences for which the sample correlation has some unknown distribution. The correlation at different lags will be drawn from the same distribution, so the peak correlation is equally likely to occur at any lag. This suggests that the distribution of peak lags should be uniform. In contrast, lagged correlations from two related sequences may be dispersed over a range of values, but the peak correlation will tend to occur at the true lag time. This result is statistical in nature, and there is no way to guarantee that the results from any particular interval are meaningful.

[24] Comparing all available GOES B_z data to ACE observations of dynamic pressure from 1998 to 2009 provided nearly 200,000 overlapping 1 h intervals suitable for shifted correlation analysis. Peak correlation delays were determined relative to the "flat" time shift $\Delta t = \Delta x/v$, using the average measured solar wind speed for each hour. If the flat time shift were the only important factor, then we might expect a delta function of tightly clustered delays and possibly also a plateau corresponding to a uniform distribution of random lags from apparently unrelated (i.e., noisy) intervals. More realistically, other effects (i.e., tilted phase planes and variations in GOES location) would likely produce a peak dispersed over some finite range of delays.

[25] For simplicity, we have calculated time shifts from ACE to a fixed location at the GSE origin. In reality, the phase planes will travel from ACE, pass through the bow shock, move through the magnetosheath, then arrive at the magnetopause, initiating compression and producing currents which generate magnetic field changes observed by GOES [*Wing et al.*, 2002]. This complicated propagation will change the arrival time at geostationary orbit, and variations in conditions will tend to further increase the apparent lag dispersion beyond that due to solar wind orientation alone. A complete detailed physics-based model of this process is, however, well beyond the scope of this study. We do note that *Wing et al.* [2002] and *Jackel et al.* [2012] both found an empirical difference in arrival times between dusk and dawn of a few minutes or less, which for the ensemble of configurations considered here should produce a corresponding overall increase in signal lag dispersion.

[26] The actual lag distribution for all events (Figure 4) has a distinct peak around $\tau = 0$, which presumably corresponds to physically meaningful correlations. The average delay is within 10 s of that predicted by flat time shifting, a result which should be considered purely fortuitous given the complexities of propagation through the magnetosheath and magnetosphere. The profile is apparently symmetric and superimposed on a plateau that falls off slightly at larger lags. Basic features are well represented with a simple model consisting of a Gaussian plus a second-order polynomial, with least-squares fitting used to determine model parameters. Roughly 12% of all intervals correspond to the Gaussian component with a peak at $\tau = –0.1$ min and a standard deviation of 6.8 min. Another 18% of events are contained in a very broad parabolic distribution also centered at zero lag. It is likely that some of these cases may correspond to more complicated solar wind configurations

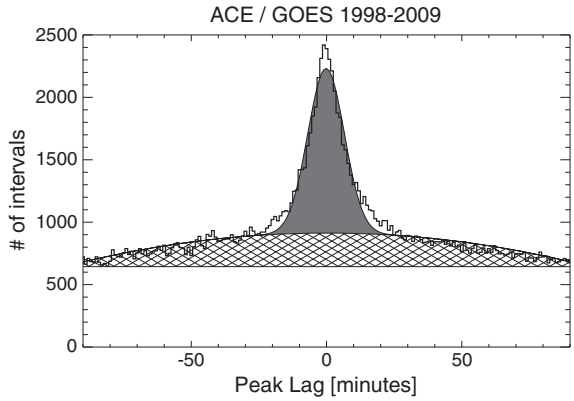

Figure 4. Distribution of peak lags relative to a "flat" ($\phi = 0$) time shift from ACE to $\vec{r}_2 = 0$ using measured solar wind speeds. Thick histogram corresponds to the observed distribution, thin line corresponds to model consisting of a Gaussian (solid shading), a second-order polynomial (cross-hatching), and a constant. The Gaussian component contains roughly 22,000 events (12% of the total).

that are not well modeled by a simple phase plane. Finally, the remaining 70% of intervals have a uniform distribution of lags as would be expected from uncorrelated processes. This apparent lack of correlation may be real but could also indicate some limitation in our analysis due to the presence of noise or other confounding physical processes (i.e., dipolarization near GOES).

[27] As can be seen in Figure 4, the Gaussian component does not always perfectly fit the lag profile peak. This effect is important when considering more complicated lag profiles that are produced for different subsets and selection criteria (see next section). We found that a reasonably robust separation of the signal peak could be obtained by first fitting the Gaussian plus polynomial model, next subtracting the polynomial contribution, then calculating moments from the residual distribution. The zeroth moment can be used to determine the fraction of intervals that fall into the narrow peak (signal fraction, denoted as f). The precise value of the first moment (average time delay $\bar{\tau}$) depends on complicated details of propagation through the magnetosheath and magnetopause; it is not used as the basis for any subsequent analysis or discussion. The standard deviation (σ) about the mean provides a measure of how widely arrival times are dispersed about some average value. Both f and σ will respond to multiple factors including solar wind orientation, post-shock propagation, and geosynchronous satellite location. In this study, we will focus on the first topic and explicitly assume that the sum of all other effects will appear as noise, which will tend to decrease f and increase σ. As such, our results may understate the effectiveness of time shifting alone.

4. Results

[28] An optimal time-shifting procedure would ideally "focus" all events to the same lag, producing an extremely narrow signal lag profile. Analysis of all intervals using a simplistic flat delay produces a more broadly dispersed baseline reference against which other more sophisticated propagation algorithms can be compared. The profile width σ and signal fraction f can be used as figures of merit to be minimized and maximized, respectively.

Table 1. Lag Profile Analysis of Data Subsets[a]

Signal Fraction	Signal Width σ (min)	# of Intervals	Constraints
12.1%	7.64	192,502	n/a
21.5%	7.75	95,448	MLT = 06–18 h
25.1%	7.43	46,580	MLT = 09–15 h
22.2%	7.03	30,831	06–18, $\|y_1\| < 20\,R_e$
21.3%	8.15	64,617	06–18, $\|y_1\| > 20\,R_e$
21.5%	6.58	26,551	06–18, $\|z_1\| < 10\,R_e$
21.7%	8.32	68,897	06–18, $\|z_1\| > 10\,R_e$
24.9%	8.86	25,239	06–18, $v < 400$ km/s
20.5%	7.35	70,209	06–18, $v > 400$ km/s

[a]The first line contains results for all data, the second for results when GOES was only on the dayside, and the third when it was within 3 h of noon. All subsequent results are with GOES on the dayside for different ranges of solar wind speeds or with ACE at different distances from the Sun-Earth line.

[29] We started by partitioning the flat delay results into different groups in order to test our expectations and the predictions of equation (3). Table 1 contains results for lag profile width and signal fraction for all events as shown in Figure 4 followed by results from subsets selected to illustrate important features.

[30] It is well known [*Wing and Sibeck*, 1997] that the effect of solar wind dynamic pressure changes are most pronounced on the dayside, due to the proximity of magnetopause currents and the distance from unrelated nightside disturbances (e.g., substorms). *Jackel et al.* [2012] also found that the majority of correlated intervals occurred within ±6 h of MLT noon. Data in this study exhibit similar behavior: the subset with GOES located on the dayside (06–18 MLT) has nearly double the signal fraction of the full data set (21% versus 12%). In other words, when a GOES satellite is located in the nightside, the probability of detecting response due to dynamic pressure forcing is very low. Further restricting GOES to within ±3 h of MLT noon increases the signal fraction only slightly to f = 25%. It is clear that the post-dawn and predusk sectors generate a large number of related intervals that can contribute to a statistical analysis. All subsequent analysis in this study will involve the larger dayside subset (06–18 MLT) in order to maximize the number of physically meaningful correlations while minimizing spurious correlations by eliminating the nightside subset.

[31] Next, we considered two sets of cases with $\Delta y \approx \leftarrow y_1$ (designated the "impact parameter" by *King and Papitashvili* [2005]) either less than or greater than 20 Re. As can be seen from equation (3), this will be the dominant correction to the direct time shift for phase-front normals near the equatorial plane ($\theta \approx$ ~~0~~) with off-radial alignment ($\phi \neq$ ~~0~~). If PFN tilts are a significant source of lag dispersion, then we would expect that larger values of y_1 would correspond to larger peak widths. This is in fact the case, with a standard deviation of 7.0 min when $|y_1| < 20R_e$, which is more than 1 min less than for $|y_1| > 20R_e$. Small offsets in GSE-z from the Sun-Earth line ($|z_1| < 10R_e$) correspond to the narrowest lag profile (σ = 6.6 min) obtained

thus far. As expected, larger offsets ($|z_1| > 10R_e$) produce a much broader profile ($\sigma = 8.3$ min).

[32] Finally, equation (3) indicates that both flat and tilted time shifts should vary inversely with solar wind speed. This suggests that faster flows should produce narrower lag profiles, while those for slower speeds should be more broadly dispersed. The last two entries in Table 1 are consistent with this prediction as σ = 8.9 min for $v < 400$ km/s and $\sigma = 7.4$ min for $v > 400$ km/s. Observed timing errors for flat propagation are larger for slow solar wind speeds.

4.1. Tilted Planes

[33] The time shift predicted by equation (2) depends on observer positions that are known, a velocity that can be plausibly inferred from single-point measurements in the solar wind, and the orientation of the phase plane which must be assumed or derived from other observations. For predominantly radial solar wind flow, the time shift can be written in a form (equation (3)) that expresses the PFN in terms of two angular parameters: ϕ ("azimuth" in the GSE-*xy* ecliptic plane) and θ ("inclination" out of the ecliptic). Many previous studies [e.g., *Richardson et al.*, 1998; *King and Papitashvili*, 2005] have assumed that the inclination angle is effectively zero, allowing the final term in equation (3) to be neglected. In this case, the time lag will depend only on the known separation in GSE-*y* and the unknown azimuth angle.

$$\tau_y \approx \frac{\Delta y}{v} \tan\phi \tag{5}$$

[34] Starting with an extremely simple model, we assumed that all PFN could be modeled as having the same nominal orientation ϕ_0. We could then identify the single "best" value of ϕ which minimized the spread of observed lag delays. The result was a clear single minimum in signal width ($\sigma = 7.3$ min) for a characteristic azimuth angle of $\phi_0 = 15°$. This angle is roughly midway between purely radial and Parker spiral orientations. This led us to ask whether the optimal tilt angle depended on solar wind speed as might be expected for the Parker spiral model. Figure 5 shows the width of the signal lag profile as a function of nominal azimuth for solar wind speeds binned in ranges 200–400, 400–600, and 600–800 km/s. As expected, the minimum is most pronounced for slow speeds and is much broader for fast speeds. However, the optimal angle is essentially the same for all three speed bins, indicating that azimuth is not a simple function of flow speed.

[35] Our next, slightly more sophisticated, approach was to use measured solar wind speeds as input to the Parker spiral model in order to predict the azimuth angle $\phi_P(v)$ for each interval. This produced a lag dispersion of almost 10 min, much worse than for either a flat delay or single nominal angle. We also considered a hybrid model

$$\phi_P = 90° + \gamma\,\alpha_P \tag{6}$$

for which $\gamma = 0$ corresponds to purely radial orientation and $\gamma = 1$ is the Parker orientation. We searched for the optimal value of γ which minimized the lag profile width. In the range 0.2–1.5, there is only a single minimum near $\gamma = 26\%$, which is generally consistent with the results for ϕ_0. However, the minimum width is only σ = 7.38 min,

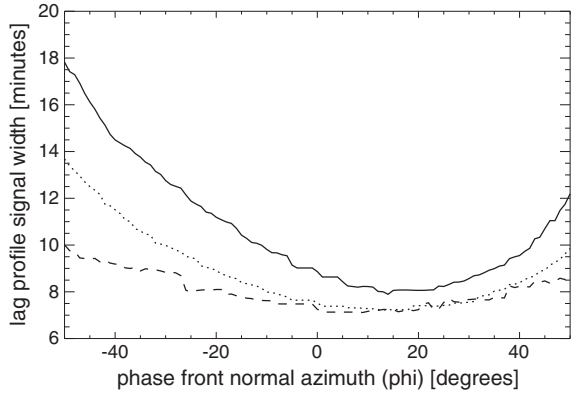

Figure 5. Signal lag profile width as a function of nominal azimuth for different solar wind speeds. Solid line corresponds to v = 200–400 km/s, dotted line 400–600 km/s, dashed line 600–800 km/s. All three cases have a single minimum located near $\phi_0 = 15°$.

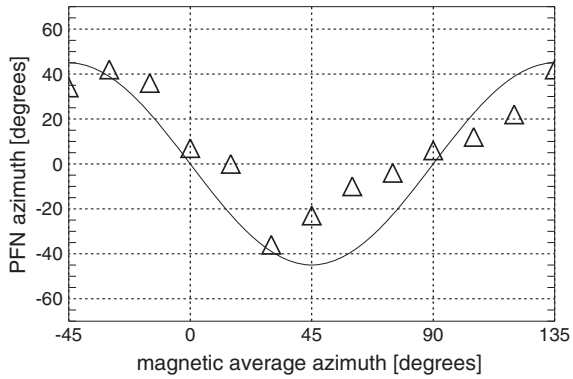

Figure 6. Optimal phase-front normal (PFN) azimuth determined using subsets grouped by average magnetic field azimuth. Symbols indicate results obtained using 30° bins. Solid line corresponds to the model in equation (7).

which is not significantly better than obtained with a single ϕ_0. The Parker spiral model does not appear to provide a useful prediction of PFN orientation in the GSE-*xy* plane.

[36] Finally, we tried using vector magnetic field orientation in order to predict PFN azimuth. ACE MFE observations of $\vec{B}$ were averaged over 1 h to determine ϕ_B corresponding to each lagged correlation analysis interval. Peak lag results were grouped according to ϕ_B in 30° wide bins from –45° to 135° (Parker spiral directions). The optimal tilt angle, corresponding to the minimum in signal peak lag width, was determined for each group. The result is a very clear relationship between magnetic field and PFN azimuth as shown in Figure 6.

[37] For the majority of cases, the interplanetary magnetic field (IMF) was aligned near the Parker spiral direction. In these cases, the optimal PFN $\hat{n}$ was oriented at right angles to $\vec{B}$. A similar relationship was found for ortho-spiral magnetic fields (perpendicular to the usual orientation) with $\vec{B} \quad \hat{n} \sim \leftarrow\theta$. For configurations where the IMF was either purely radial or aligned with GSE-*x*, the

optimal PFN vectors were aligned in the GSE-x direction. There also appears to be a smooth transition through all intermediate IMF orientations between these four limiting cases. Equation (7) presents a purely heuristic model for the relationship between ϕ_B and $\phi_{\hat{n}}$ that is extremely simple

$$\phi_{\hat{n}} = -45^\circ \sin(2\,\phi_B) \tag{7}$$

and produces a good fit to observations as shown in Figure 6. Some physical implications of this model are addressed in section 5.

4.2. Inclined Planes

[38] In general, it is necessary to consider the possibility that phase-front normals do not always lie in the GSE-xy plane. If the PFN inclination angle θ is not zero, then there may be an additional time shift from the third term of equation (3). The magnitude of this correction depends on the azimuth, inclination, and the ratio of GSE-z offset to solar wind velocity. Previous studies [e.g., *Richardson et al.*, 1998; *King and Papitashvili*, 2005] have tended to neglect this Δz effect. One reasonable justification for concentrating on the Δy term is that recent L1 probes have tended to utilize orbits for which $\Delta z \sim \frac{1}{2}\Delta y$. However, if the inclination angles are sufficiently large, then it is possible that the third term in equation (3) may be important even for small GSE-z offsets.

[39] We can explore this issue by binning with respect to ACE lateral position (y_1 and z_1), with the results presented in Table 2. Offsets in GSE-y range from 0 to 50 Re, while those in GSE-z are roughly half as large (0 to 30 Re). The signal peak width is narrowest for the smallest offsets, as expected from equation (3), and the peak width increases with increasing $|y|$. The flat-lag dispersion also becomes larger with increasing $|z|$, indicating that the inclination effect is in fact significant.

[40] The increase in width is roughly linear for increasing offset with similar trends ($\sim$0.1 min/Re) in both the y and z directions. Such a linear dependence in lateral (y or z) offset is consistent with the form of equation (3). The second and third (nonflat) terms appear to be of roughly equal importance for similar offsets

$$\left|\frac{\Delta y}{v}\tan\phi\right| \approx \left|\frac{\Delta z}{v}\frac{\tan\theta}{\cos\phi}\right|, \quad |\Delta y| \approx |\Delta z| \tag{8}$$

giving a simple relationship between characteristic values for the azimuth and inclination

$$|\sin\phi| \approx |\tan\theta| \tag{9}$$

For example, if all phase planes were tilted with the Parker spiral ($\phi = -45^\circ$), then they would also have to be at significant inclinations ($\theta = \pm 35^\circ$) to produce the observed patterns in observed lag width.

Table 2. Standard Deviation (σ, in Minutes) of Lag Profile Peak Width for Flat Delays Binned by ACE Offset From GSM-y,z = 0[a]

	GSE $\|y\|$				
GSE $\|z\|$	0–10	10–20	20–30	30–40	40–50
0–10	4.93	5.39	5.58	7.35	8.80
10–20	5.71	6.80	8.05	8.65	9.17
20–30	8.71	7.83	8.08	8.90	9.40

[a]Increase in width with offset is symmetric in GSE-y and GSE-z and approximately linear with an intercept of 4.5 min.

5. Discussion and Conclusions

[41] Using upstream observations to predict solar wind conditions near the Earth is typically accomplished using a simple model of convecting phase planes structures. Model parameters include several quantities that are well known as a function of time, such as spacecraft location and solar wind speed. The phase-front normal orientation also plays a critical role but is more difficult to determine from short data intervals. Previous studies have used similar observations from two or more satellites in the solar wind to explore features of large-scale structures. In this paper, we have used the physical relationship between solar wind dynamic pressure and geosynchronous B_z to assemble a very large set of correlated intervals. These results allow a detailed examination of phase-front orientation.

[42] We start with the expectation that for $\Delta y = \Delta z = 0$ the signal lag profile width (standard deviation) will be very narrow because the time shift should not depend on PFN orientation. Of course, some scatter is inevitable when attempting to correlate two noisy time series at 1 min resolution. Additional spread may be produced by the complicated transfer function (i.e., low-pass filter) relating dynamic pressure to geosynchronous magnetic fields. Travel times from the bow shock to geosynchronous orbit can also vary by several minutes depending on GOES location, resulting in further broadening. Some fraction of the nonzero dispersion could be due to physics not included in our model (i.e., temporal evolution), but it is not clear how this could be separated from other effects.

[43] Considering only the subset of cases with small lateral offsets did produce the smallest observed dispersion (just below 5 min) as expected. The dispersion for larger lateral offsets should in principle be the same (or larger) even if perfect corrections for azimuth and inclination effects could somehow be determined. A practical upper limit of 7.8 min is given by the flat lag τ_{yz} for all events. On average, the simplest propagation algorithm is only 3 min worse than the best case outcome.

[44] These results are generally consistent with those from previous studies. *Collier et al.* [1998] compared Wind and IMP-8 magnetic fields and found 66% of good correlation events with better than 10 min accuracy, with the caveat that only 12% of their 543 intervals qualified as "good." *Ridley* [2000] used a few hundred carefully selected IMP-8 and Wind magnetic field intervals and found timing errors in the 2–6 min range for small lateral offsets and errors of roughly 8 min for offsets of 30 Re. *Mailyan et al.* [2008] compared several hundred intervals of magnetic field data from ACE and Cluster and found timing errors in the 5–10 min range. Comparing two different quantities (P_d and B_z) seems to give results that agree with those obtained from direct comparisons of magnetic field.

[45] The error for each individual case will likely depend on a combination of the relative offsets and the PFN orientation. Taking advantage of our very large number of events, we were further able to bin events in both Δy and Δz. This allows us to separate the effects of lateral offsets from the

Sun-Earth line. For each row of Table 2, GSE-z is constant and the dispersion increases with GSE-z. A linear fit to the trend

$$\sigma = a\,\Delta y + b\,\Delta z \tag{10}$$

gives a similar slope for each row: a = 0.1 min/Re. This value should scale as $\tan\phi/v$, so assuming an average solar wind speed of 400 km/s would result in a characteristic azimuth of $\tilde{\phi} \sim$ ~~2~~0°. A similar linear trend is apparent for each column of Table 2, showing the importance of GSE-z offsets as a source of timing errors. Determining a characteristic value for inclination from the average velocity and characteristic azimuth gives $\tilde{\theta} \sim$ ~~2~~0°. These very rough estimates indicate that if the typical PFN is tilted midway between purely radial and the Parker spiral angle, then it must also often be significantly inclined with respect to the equatorial plane.

[46] A more detailed understanding of how θ and ϕ vary on a case-by-case basis cannot be obtained using a statistical approach. Some progress can however be accomplished by making the simplifying assumption that $\theta \approx$ ~~0~~. Admittedly, we have just finished showing that inclination effects are not negligible, but this approximation is ubiquitous in many previous studies [e.g., *Richardson and Paularena*, 1998; *Ridley*, 2000; *March et al.*, 2005]. One physical justification is that we expect PFN inclination to be symmetrically distributed about the equatorial plane, so the $\tan\theta$ term in equation (3) should average to zero. Another argument is the roughly 2 : 1 ratio of Δy : Δz for the ACE orbit, which gives a higher weighting to the $\tan\phi$ term in equation (3). However, the fundamental motivation for neglecting inclination is simply that the problem reduces to a single variable: azimuth ϕ.

[47] As shown in Figure 5, the signal lag profile width has a clear single minimum near $\phi_0 \approx$ ~~1~~5°. This does not mean that all PFN are tilted in that direction, but it does indicate that the distribution of tilt angles is not completely uniform. In the absence of any other information about PFN orientation, the optimal approach would be to propagate all solar wind data assuming a characteristic angle of ϕ_0.

[48] Our results are consistent with those obtained from previous studies. A correlation analysis by *Richardson and Paularena* [1998] used solar wind density and magnetic fields from WIND/ISEE-3 and IMP-8 to find orientations in the range 13° to 36°. It should be noted that their results were obtained from the dominant subset of "6-hour time periods where the average magnetic field was within 45° of the average Parker spiral angle at Earth of 45°," but ours also include all other orientations.

[49] It is surprising that more complex Parker scaled models fail to significantly reduce lag dispersion. Of course, the Parker spiral is a large-scale model that does not include any turbulent effects, but the general pattern is obvious in Figure 1. We had expected that solar wind speed would thus have some value for predicting PFN azimuth. This does not appear to be the case at least for the analysis method used in this study.

[50] One-hour averages of the magnetic field direction do however appear to provide a useful predictive capacity. If there was no useful information in the magnetic field direction, then the same characteristic tilt angle ϕ_0 should be obtained for any subset of intervals. It is evident from Figure 6 that grouping intervals in terms of ϕ_B produces a clear pattern of variation in $\phi_{\hat{n}}$. Four representative configurations are shown in Figure 7. In three of these cases, the PFN is oriented at right angles to the magnetic field vector so that each field line lies in the plane of constant phase. These geometries are all consistent with the same basic model, where spatial variations near the Sun produce solar wind structures that are roughly uniform along a field line but may vary considerably between flux tubes. In the fourth case, magnetic field lines are directed radially away from the Sun and parallel to the PFN vector. This would presumably correspond to temporal variations in plasma flow along a single flux tube. Our attempt at expressing all four relationships in a simple model (equation (7)) is admittedly not derived from fundamental plasma physics but does clearly succeed in providing a very good fit to observed trends.

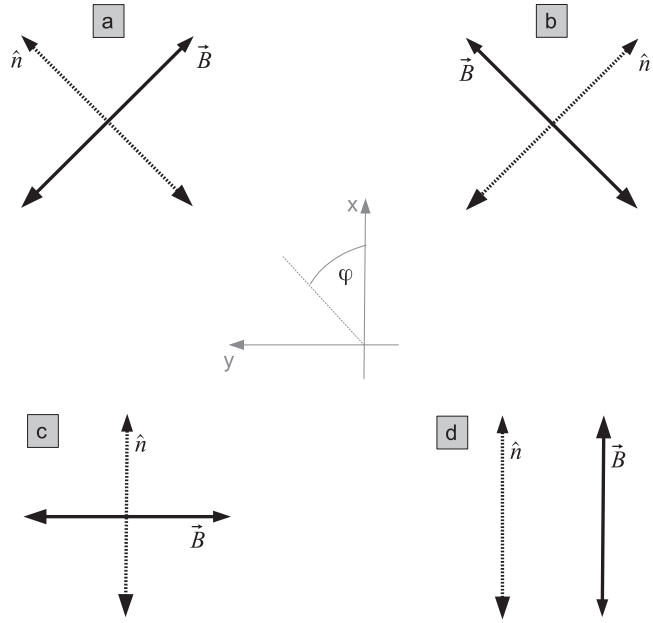

Figure 7. Relationship between magnetic field and phase-front normal orientation (a) typical Parker spiral magnetic field, (b) less common "ortho-spiral" configuration, (c) intermediate azimuthal field, (d) intermediate radial field. $\vec{B}$ $\hat{n} \approx$ ~~0~~ for cases in Figures 7a–7c.

[51] Previous studies have used hundreds of events to determine averages of important quantities such as PFN azimuth angle $\phi_{\hat{n}}$. By working with tens of thousands of intervals, we have been able to consider joint statistics, beginning with exploration of how $\phi_{\hat{n}}$ depends on the average magnetic field orientation. A similar approach could be used to study the effectiveness of different minimum variance techniques currently employed for predicting PFN orientation.

[52] Having more intervals for comparison would obviously improve the statistical power of future studies. One approach would be to simply include data from more satellites. Considering the Wind spacecraft would nearly double the number of solar wind observations near L1. THEMIS probes might also provide an additional measure of magnetospheric response, albeit not at relatively well-understood geosynchronous orbits. In theory, any combination (past, present, or future) of simultaneous solar wind pressure and

near-Earth magnetic field observations could be used. A complementary approach would be to try improving our ability to detect causal relationships in the existing data. The signal fraction detected with fairly simple correlation analysis of all intervals was roughly 12%. Even a 1% improvement would add 2000 more intervals, which would be a significant increase.

[53] This novel application of the relationship between solar wind dynamic pressure and geosynchronous magnetic field provides a very promising method for studying solar wind structure and orientation. We have been able to replicate and expand upon some previously published results and to discover a new empirical relationship between phase-front normal azimuth and average magnetic field. In the future, using an expanded data set will allow us to refine our results and extend our analysis to a quantitative comparison of PFN estimators, possibly leading to an improved understanding of solar wind structure orientation and propagation.

Appendix A: Moving Phase Plane

[54] A plane can be completely defined in terms of one point in the plane $(\vec{r}_0)$ and a normal to the plane ($\hat{n}$). The vector difference between $\vec{r}_0$ and any other point in the plane $(\vec{r})$ must by definition be perpendicular to the normal

$$\hat{n} \quad (\vec{r} - \vec{r}_0) = 0 \tag{A1}$$

For the solar wind problem, we are interested in finding when a moving tilted phase plane which first passes over a single point will later arrive at some other reference point (e.g., the bow shock or a second satellite). This gives an implicit equation for the intersection time t_0

$$\hat{n} \quad [\vec{r}_2(t_0) - \vec{r}_1(t_0)] = 0 \tag{A2}$$

where $\vec{r}_1(t)$ is a point moving with the plane at velocity $\vec{v}$ and $\vec{r}_2(t)$ is the trajectory of the second observer. If the plane velocity is constant, then

$$\hat{n} \quad [\{\vec{r}_2(t_2)\} - \{\vec{r}_1(t_1) + \vec{v}\Delta t\}] = 0 \tag{A3}$$

where $\Delta t = t_2 - t_1$ is the time delay between initial and secondary observations. Rearranging terms gives a general result

$$\Delta t = \frac{[\vec{r}_1 - \vec{r}_2] \quad \hat{n}}{\vec{v} \quad \hat{n}} = \frac{\Delta\vec{r} \quad \hat{n}}{\vec{v} \quad \hat{n}} \tag{A4}$$

At this point, it is useful to express the plane normal using spherical coordinates

$$\hat{n} = \cos\theta\cos\phi\,\hat{x} + \cos\theta\sin\phi\,\hat{y} + \sin\theta\,\hat{z} \tag{A5}$$

where azimuth $\phi = 180°$ and inclination $\theta = 0$ corresponds to antisunward flow. If the phase plane is embedded in the solar wind which has a bulk motion that is almost entirely antisunward, then $\vec{v} \approx \leftarrow\!\!\!| v\hat{x}$ and the time shift in terms of the offset between the two observation locations ($\Delta x = x_2 - x_1$, $\Delta y = y_2 - y_1$, $\Delta z = z_2 - z_1$)

$$\Delta t \approx \frac{\Delta x\cos\theta\cos\phi + \Delta y\cos\theta\sin\phi + \Delta z\sin\theta}{-v\cos\theta\cos\phi} \tag{A6}$$

reduces to

$$-\Delta t \approx \frac{\Delta x}{v} + \frac{\Delta y}{v}\tan\phi + \frac{\Delta z}{v}\frac{\tan\theta}{\cos\phi} \tag{A7}$$

In this paper, we consider the distribution of lags for solar wind data that have only been "flat" shifted

$$\tau_{yz} = -\Delta t - \frac{\Delta x}{v} \approx \frac{\Delta y}{v}\tan\phi + \frac{\Delta z}{v}\frac{\tan\theta}{\cos\phi} \tag{A8}$$

in order to study the effects due to lateral offset and phase plane orientation.

[55] **Acknowledgments.** T. Cameron was supported by funds from the Canadian Natural Sciences and Engineering Research Council (NSERC). GOES magnetometer data were produced by NOAA/SWPC and obtained from CDAWeb. ACE solar wind data were produced by the MAG (PI: N. Ness at Bartol Research Institute) and SWE (PI: D. J. McComas at Southwest Research Institute) teams and obtained from CDAWeb.

References

Blanchard, G. T., and D. Bankston (2002), Improved interplanetary magnetic field propagation timing by correction of the phase front orientation using two spacecraft, *J. Geophys. Res.*, *107*(A12), 2–5, doi: 10.1029/2002JA009258.

Collier, M. R., J. A. Slavin, R. P. Lepping, A. Szabo, and K. Ogilvie (1998), Timing accuracy for the simple planar propagation of magnetic field structures in the solar wind, *J. Geophys. Res.*, *25*(14), 2509–2512.

Jackel, B. J., B. McKiernan, and H. Singer (2012), Geostationary magnetic field response to solar wind pressure variations: Time delay and local time variation, *J. Geophys. Res.*, *117*(A5), doi:10.1029/2011JA017210.

Kelly, T. J., N. U. Crooker, G. L. Siscoe, C. T. Russell, and E. J. Smith (1986), On the use of a sunward libration-point-orbiting spacecraft as an interplanetary magnetic field monitor for magnetospheric studies, *J. Geophys. Res.*, *91*(A5), 5629–5636.

Kepko, L., H. Spence, and H. Singer (2002), ULF waves in the solar wind as direct drivers of magnetospheric pulsations, *Geophys. Res. Lett.*, *29* (8), 1–4, doi:10.1029/2001GL014405.

King, J., and N. Papitashvili (2010), *One min and 5-min solar wind data sets at the Earth's bow shock nose*. http://omniweb.gsfc.nasa.gov/html/HROdocum.html.

King, J. H., and N. Papitashvili (2005), Solar wind spatial scales in and comparisons of hourly Wind and ACE plasma and magnetic field data, *J. Geophys. Res.*, *110*(A02104), doi:10.1029/2004JA010649.

Lepping, R., C.-C. Wu, and K. McClernan (2003), Two-dimensional curvature of large angle interplanetary MHD discontinuity surfaces: IMP-8 and WIND observations, *J. Geophys. Res.*, *108*(A7), 1–20, doi: 10.1029/2002JA009640.

Mailyan, B., C. Munteanu, and S. Haaland (2008), What is the best method to calculate the solar wind propagation delay? *Ann. Geophys.*, *26*, 2383–2394.

March, T., S. Chapman, and R. Dendy (2005), Mutual information between geomagnetic indices and the solar wind as seen by Wind: Implications for propagation time estimates, *Geophys. Res. Lett.*, *32*, 1–4, doi: 10.1029/2004GL021677.

McComas, D. J., S. J. Bame, P. Barker, W. Feldman, J. Phillips, P. Riley, and J. W. Griffee (1998), Solar wind electron proton alpha monitor (SWEPAM) for the Advanced Composition Explorer, *Space Sci. Rev.*, *86* (1), 563–612.

Ogilvie, K., M. Coplan, D. Roberts, and F. Ipavich (2007), Solar wind structure suggested by bimodal correlations of solar wind speed and density between the spacecraft SOHO and Wind, *J. Geophys. Res.*, *112*(A08104), 563–612.

Parker, E. (1965), Dynamical theory of the solar wind, *Space Sci. Rev.*, *4* (5), 666–708.

Richardson, J., and K. Paularena (1998), The orientation of plasma structure in the solar wind, *Geophys. Res. Lett.*, *25*, 2097–2100.

Richardson, J., F. Dashevskiy, and K. Paularena (1998), Solar wind plasma correlations between L1 and Earth, *J. Geophys. Res.*, *103*, 14,619–14,629.

Ridley, A. (2000), Estimations of the uncertainty in timing the relationship between magnetospheric and solar wind processes, *J. Atmos. Sol. Terr. Phys.*, *62*, 757–771.

Singer, H., L. Matheson, R. Grubb, A. Newman, and S. Bouwer (1996), Monitoring space weather with GOES magnetometers, *SPIE Proceedings*, *vol. 2812,* Denver, Colo.

Siscoe, G., V. Formisano, and A. Lazarus (1968), Relationship between geomagnetic sudden impulses and solar wind pressure changes—an experimental investigation, *J. Geophys. Res.*, *73*(15), 4869–4874.

Smith, C. W., J. L'Heureux, N. F. Ness, M. H. Acuña, L. F. Burlaga, and J. Scheifele (1998), The ACE magnetic fields experiment, *Space Sci. Rev.*, *86*(1), 613–632.

Stone, E. C., A. M. Frandsen, R. A. Mewaldt, E. R. Christian, D. Margolies, J. F. Ormes, and F. Snow (1998), The advanced composition explorer, *Space Sci. Rev.*, *83*(1), 1–22.

Weimer, D., D. Ober, N. Maynard, W. Burke, M. Collier, D. McComas, N. Ness, and C. Smith (2002), Variable time delays in the propagation of the interplanetary magnetic field, *J. Geophys. Res.*, *107*(A8), doi: 10.1029/2001JA009102.

Weimer, D. R., and J. H. King (2009), Improved calculations of interplanetary magnetic field phase front angles and propagation time delays, *J. Geophys. Res.*, *113*, 1–14, doi:10.1029/2007JA012452.

Wing, S., and D. G. Sibeck (1997), Effect of interplanetary magnetic field *z* component and the solar wind dynamic pressure on the geosynchronous magnetic field, *J. Geophys. Res.*, *102*(A4), 7207–7216.

Wing, S., D. G. Sibeck, M. Wiltberger, and H. Singer (2002), Geosynchronous magnetic field temporal response to solar wind and IMF variations, *J. Geophys. Res.*, *107*, 1–10, doi:10.1029/2001JA009156.